Available online at www.sciencedirect.com
SCIENCE DIRECT
Polymer 46 (2005) 429–437
polymer
www.elsevier.com/locate/polymer

Structure and thermal molecular motion at surface of semi-crystalline isotactic polypropylene films

Atsushi Sakai, Keiji Tanaka*, Yoshihisa Fujii, Toshihiko Nagamura, Tisato Kajiyama*

Department of Applied Chemistry, Faculty of Engineering, Kyushu University, 6-10-1 Hakozaki, Higashi-ku, Fukuoka 812-8581, Japan

Received 15 July 2004; received in revised form 8 November 2004; accepted 10 November 2004

Abstract

Surface crystalline structure in isotactic polypropylene (iPP) films was explored by in-plane grazing incidence X-ray diffraction measurement. Apparent crystallinity in the surface region was lower than the bulk one. After an etching treatment with a droplet of potassium permanganate solution, a clear crater was formed at the surface, and the step height between etched and intact regions was approximately 3 nm. This means that the iPP surface was covered with 3 nm thick amorphous layer. Then, surface molecular motion in the iPP films was examined by lateral force microscopy. Surface α_a-relaxation process arisen from the segmental motion was observed at about 250 K, and its apparent activation energy was 230 ± 10 kJ mol^{-1}. The both were lower than the corresponding bulk values, indicating that surface molecular motion is more active than the bulk one even in the semi-crystalline iPP films. An iPP film with 1.5 nm thick surface amorphous layer was prepared. In this case, the enhanced mobility was still observed at the surface, but the extent of the enhancement was not remarkable as that for the iPP film with 3 nm thick surface amorphous layer. These results imply that surface mobility is affected by the presence of underneath crystalline phase, if the surface amorphous layer is thin enough.

Keywords: Surface aggregation structure; Surface molecular motion; Isotactic polypropylene (iPP)

1. Introduction

Surfaces of polymeric materials play an important role in many technological applications. To design highly functionalized polymeric materials, the systematical understanding of structure and physical properties in the vicinity of surface, which are impossible to be deduced only by extrapolating its bulk ones, is of pivotal importance as the first benchmark. So far, many experimental techniques have been already established for surface structure, and knowledge emerged has been utilized in designs for liquid repellency, biocompatibility, adhesion, and so forth [1,2]. However, this is not the case for surface physical properties of polymers, because the field has been just opened recently.

In the last decade, surface molecular motion in amorphous polymer films has been studied with the advent of modern experimental techniques. Consequently, major conclusion emerged so far is that surface mobility is more enhanced than the internal bulk one [3–18], although some contradict arguments have been going on [19–21]. To understand precisely how surface mobility differs from the bulk one, systematic studies are necessary. In addition, it should be confirmed whether a notion of the enhanced surface mobility is universal even for semi-crystalline polymers.

Considering a mass consumption of polymers in industry, semi-crystalline polyolefin can be regarded as one of most important polymers due to its excellent cost performance [22]. Surface aggregation states in films of isotactic polypropylene (iPP) and low and high density polyethylene (LDPE and HDPE) have been studied by scanning force microscopy (SFM) [23–25] and surface sensitive scattering techniques [26–28]. Of the scattering methods, grazing incidence X-ray diffraction (GIXD) measurement enables us to gain direct access to crystalline structure such as crystallinity, orientation and packing structure, in the surface region [29,30]. To date, many

* Corresponding authors. Tel.: +81 92 642 3560 (K. Tanaka); +81 92 642 2100 (T. Kajiyama); fax: +81 92 651 5606.
E-mail addresses: k-tanaka@cstf.kyushu-u.ac.jp (K. Tanaka), kajiyama@cstf.kyushu-u.ac.jp (T. Kajiyama).

0032-3861/$ - see front matter © 2004 Elsevier Ltd. All rights reserved.
doi:10.1016/j.polymer.2004.11.021

discrepancies of crystalline structure between surface and bulk have been reported for iPP, LDPE and HDPE [26–28], provided that specimens used were mostly compression-molded to decrease surface roughness [26,27]. On the other hand, a little information has been known on surface molecular motion in semi-crystalline polymer films for the moment. Gracias et al. have examined glass transition temperature (T_g) at the iPP surface by SFM in conjunction with sum-frequency vibrational spectroscopy, and concluded that there is no appreciable T_g difference between surface and bulk [31]. Uedono et al., using positron annihilation spectroscopy, have also claimed that molecular motion in the sub-surface region of iPP films is frozen unless temperature goes beyond the bulk T_g [32]. However, since this experiment analyzed the depth region of 200 nm, which was much deeper than usual surface sensitive techniques, it is no wonder that they have not seen any signatures of enhanced mobility in the sub-surface region. In contrast, Kawamoto and co-workers have tried to extract surface molecular motion in compression-molded iPP films with different surface crystallinity on the basis of dynamic mechanical analysis, and successfully presented that the segmental motion in the surface region is thermally vigorous compared with that in the bulk [33]. As seen in the above reports, there exist controversial arguments for surface mobility in semi-crystalline polymers as well. Thus, more experimental data should be collected to clarify the issue.

The objective of this study is to reveal aggregation structure and molecular motion in the surface region of iPP films by GIXD measurement and lateral force microscopy, and to combine them. Information so obtained is compared with what we have learned from the surface of amorphous polymers [5]. This would be quite helpful to perceive characteristics of polymer surfaces.

2. Experimental section

2.1. Materials and film preparation

Sample used in this study was an additive free iPP (MFR = 10 g $(10\ \text{min})^{-1}$), which was kindly supplied by Japan Polychem Corporation. Films with the thickness of approximately 170 nm and 1 mm were prepared on Si wafers with a native oxide layer, as follows. Since our goal has been to understand characteristics of pristine polymer surface, we restricted ourselves to not use compression-molded samples, although it was better to be used in terms of decreasing surface roughness. The thin film was prepared by a spin-coating method from 1.6 wt% *p*-xylene solution. The solution used was heated up to the boiling temperature of *p*-xylene under N_2 atmosphere, and was cast onto the substrate kept to be 393 K. In the case of the thick film, iPP powders were simply melted on the substrate at approximately 473 K in vacuo. Finally, both thin and thick films were melted at 473 K under N_2 atmosphere and quenched to 273 K using iced water. Root-mean-square (RMS) roughness of the thin and thick films was about 3 and 10 nm, respectively. The bulk T_g (T_g^b) of the thick film was determined to be 267 K by dynamic mechanical analysis, and the bulk crystallinity was 53% by wide angle X-ray diffraction (WAXD) measurement. In addition, an iPP film was prepared by a different procedure as described below. First, iPP powders were cast on a Si wafer, and were melted at 473 K under N_2 atmosphere. Then, a NaCl crystal with cleaved fresh surface was put on it. Finally, it was immediately immersed into an iced water bath to dissolve NaCl as well as to quench the film. Hereafter, the film obtained is abbreviated as iPP-NaCl. WAXD measurement revealed that the bulk crystallinity of the iPP-NaCl film was the same as that of the iPP film within our experimental accuracy.

2.2. Surface structure

When the surface crystalline structure is examined by in-plane measurement of GIXD, the sample surface should be as flat as possible because an angle at which X-rays undergo total external reflection is dependent on the surface roughness. Thus, the 170 nm thick iPP film with the roughness less than that of the thick one was used. A graphite-monochromatic Cu Kα radiation ($\lambda = 0.1542$ nm) was used as the incident beam, generated by an RU-300 X-ray generator (Rigaku Ltd, Co.) at 50 kV and 250 mA. The sample was placed on the stage of a four-axis diffractometer (RINT in-plane goniometer, Rigaku Ltd, Co.). When the incident angle (α_i) of X-rays to the sample surface is equal to, or smaller than, the critical angle (α_c), the incident X-rays undergo total external reflection and penetrate into the sample as evanescent waves. The penetration depth of evanescent X-rays changes, from a few nanometers to several micrometers, depending on the α_i [29]. The α_c value is given by

$$\alpha_c = (\lambda^2 r_e N/\pi)^{1/2} \tag{1}$$

where λ is wavelength of X-rays, r_e is classical electron radius and N is electron density per unit volume of materials. The α_c of iPP was calculated to be 0.148° for $\lambda = 0.1542$ nm. Hence, the measurements were made at $\alpha_i = 0.13$ and 0.20° for surface and bulk, respectively, in this study. The penetration depth (d_p) of evanescent waves can be expressed by the following equations depending on whether the α_i is larger or smaller than the α_c.

$$d_p = \frac{1}{\sqrt{2}k\left\{\sqrt{(\alpha_c^2 - \alpha_i^2)^2 + 4\beta^2} + \alpha_c^2 - \alpha_i^2\right\}^{1/2}} \quad (\alpha_i < \alpha_c) \tag{2.1}$$

$$d_p = \frac{\sin \alpha_i}{\mu} \quad (\alpha_i > \alpha_c) \tag{2.2}$$

where k is wave vector, β is defined as $\mu\lambda/4\pi$ and μ is linear absorption coefficient. The ideal d_p at $\alpha_i = 0.13$ and 0.20° were 10 nm and 9.6 μm, respectively. Reflection from crystalline planes in the samples was detected with a scintillation counter scanned in the in-plane direction. In such, scattering vector can be regarded as parallel to the sample surface. The time for the data collection was 300 s per a step, and the angular interval between steps was 0.02°.

Amorphous phase in the surface region was tried to strip off by putting a droplet of potassium permanganate ($KMnO_4$) solution onto the film. $KMnO_4$ solution has been widely accepted to be effective to dissolve selectively amorphous region [34]. The etching solution was prepared by dissolving $KMnO_4$ into a mixed solution of phosphoric acid, sulfuric acid and water. To change the strength of the solution, the mixing ratio was adequately changed. Table 1 shows the weight ratio of ingredients in the $KMnO_4$ etchants. Surface morphology of the iPP films was observed by atomic force microscopy (AFM, SPA 300, Seiko Instruments Industry Co., Ltd) with an SPI 3700 controller. The calibration for a piezoelectric scanner was made using both silicon gratings with the height difference of 22 nm and silicon crystalline (111) plane with 0.31 nm step. A cantilever with a bending spring constant of 0.11 ± 0.02 N m^{-1}, of which both sides were coated by gold, was used. Radius of curvature of tips was 42.8 ± 2.6 nm.

2.3. Surface molecular motion

Surface relaxation behavior in the iPP films was examined by lateral force microscopy (LFM, SPA 300 HV, Seiko Instruments Industry Co., Ltd) with an SPI 3800 controller. LFM measurements were carried out at the heating rate of 0.4 K min^{-1} in vacuum so as to avoid the surface oxidation and the capillary force effect induced by surface-adsorbed water. It has been pre-confirmed by AFM that the surface was not damaged under this experimental condition. Molecular motion of a bulk iPP sample was also measured using Rheovibron (DDV01-FP, Orientec Co., Ltd) at the heating rate of 1 K min^{-1}.

3. Results and discussion

3.1. Surface aggregation structure

First of all, surface crystalline structure in a 170 nm thick iPP film was examined by in-plane GIXD measurement. Fig. 1 shows diffraction patterns for the iPP film, acquired at $\alpha_i = 0.13$ and 0.20°. Since the ideal penetration depths with $\alpha_i = 0.13$ and 0.20° were 10 nm and 9.6 μm, respectively, the measurements at $\alpha_i = 0.13$ and 0.20° could reveal crystalline structure in the surface and bulk regions. Diffraction patterns obtained from both surface and bulk regions were typical ones as the α-form of the iPP crystal. The profiles were dissolved into five diffraction peaks and a diffuse scattering come up with amorphous phase, as shown in Fig. 1, and then, crystallinity was calculated on the basis of Natta's method [35]. The value obtained at $\alpha_i = 0.13°$ was 43.6%, which was smaller than the corresponding bulk value of 51.0% at $\alpha_i = 0.20°$. In the GIXD measurement, scattering vector was along the direction parallel to the surface, meaning that the crystalline lattice plane normal to the surface was monitored. Hence, it should be careful that crystallinity obtained by this method was not necessarily real but apparent, although the essential discussion about the depressed crystallinity in the surface region would not be altered. This conclusion was in qualitative agreement with independent reports by Kawamoto et al. [26] and Nishino et al. [27] using compression molded iPP films.

Based on the GIXD results, it is clear that the surface fraction of amorphous phase is higher than the bulk one. To address how the amorphous phases distribute in the surface region, a droplet of $KMnO_4$ solution was put onto iPP films with the thickness of approximately 1 mm [36]. After a given time, the droplet was taken away and the surface was carefully washed with a large amount of pure water. Fig. 2 shows surface morphology for the iPP film, especially focusing on the boundary between intact and etched regions, and height profile along the line in the topographic image. For this observation, etchant B was used, and 30 min was allowed to dissolve surface amorphous phase. The area treated by the etchant, corresponding to the left-hand side in the AFM image, was lower than the intact region in height. Actually, a crater was formed at the surface after the etching treatment. This result makes it clear that the surface in the iPP film was mostly covered with an amorphous layer. When an etching solution with adequate oxidation ability is used, the surface amorphous layer will be well removed. However, if the etching condition is ill-chosen, underneath crystalline phase is in part corroded, or the surface amorphous phase is left, resulting in an incorrect estimation of the thickness of the surface amorphous layer. Hence, the solution concentration and the etching time were systematically varied to find an optimized etching condition. Fig. 3

Table 1
Weight ratio of ingredients in $KMnO_4$ etchants

Etchant	H_3PO_4	H_2SO_4	H_2O	$KMnO_4$
A	30	20	50	0.25
B	40	27	33	0.33
C	45	30	25	0.38
D	23	63	14	1.00

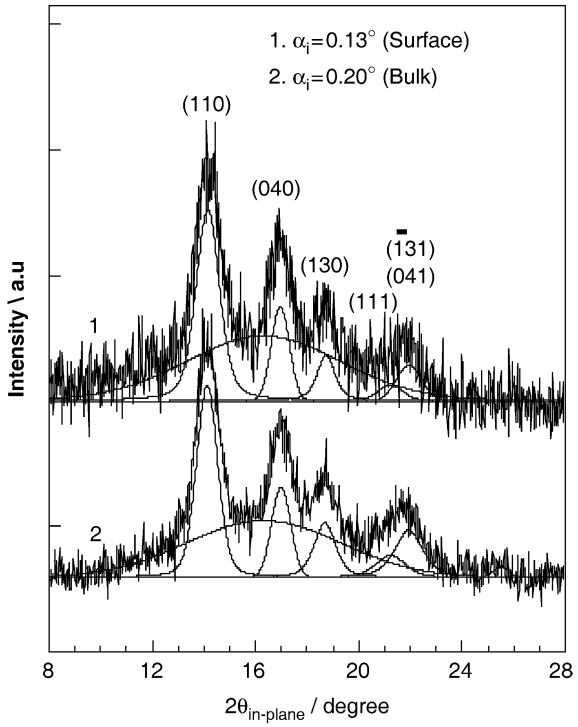

Fig. 1. In-plane GIXD profiles from surface and bulk in the iPP film.

shows the etching time dependence of height difference between etched and intact regions on the iPP film using various etchants. As a weak condition was chosen, the surface oxidation was not detectable. This was the case for etchants A, B and C for short time within a few minutes. When these etchants were used for 5 min, the surface was definitely etched and the height difference became to be in the range of 2.5–3 nm. In the case of the etching treatment for a time longer than 10 min, the height difference remained an almost constant of approximately 3 nm. These results show that the amorphous phase was gradually removed from the surface by the permanganate solution until it was completely taken away. Postulating that the height difference between the two regions corresponds to the thickness of the surface amorphous layer, the value was estimated to be 3.3 ± 0.4 nm. Once the etchant D being the strongest in this study was used for 60 min., the crystalline phase beneath the amorphous layer was partially eroded. Then, the surface layer thickness was overestimated to be about 8 nm.

For the sake of completeness for our discussion about surface aggregation states in the iPP films, the results obtained after the etching treatment are compared with the GIXD results. As mentioned before, the ideal penetration depth of evanescent waves, which would correspond to the analytical depth, for GIXD was 10 nm for the grazing angle of 0.13°. In that case, the crystallinity obtained was 43.6%. We now assume a simple bilayer-like structure in the surface region, in which the amorphous layer is present on the bulk phase with the crystallinity of 51.0%. Taking into

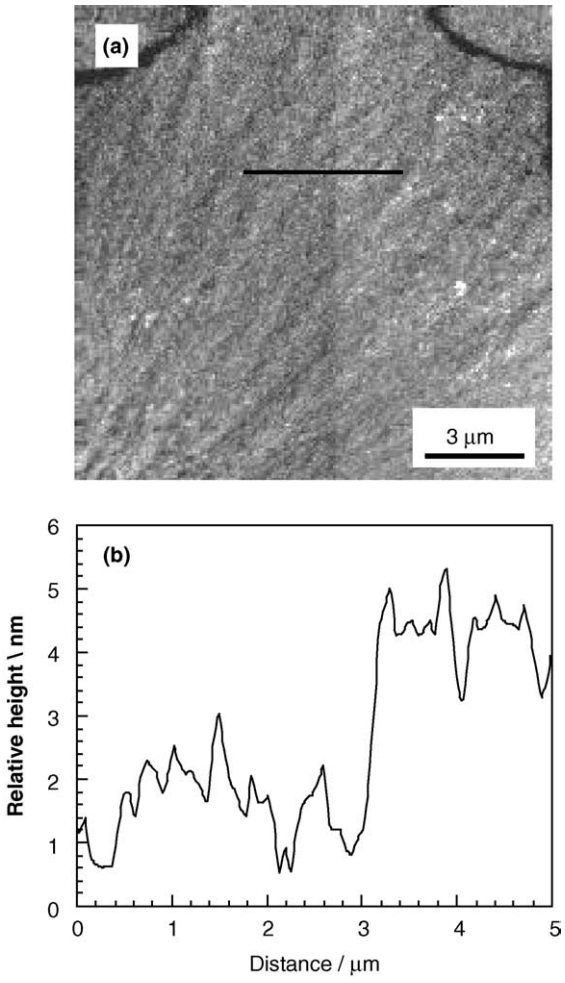

Fig. 2. (a) Topographic image for the iPP film surface, which was partially oxidized by permanganate solution, and (b) height profile along the line in the image.

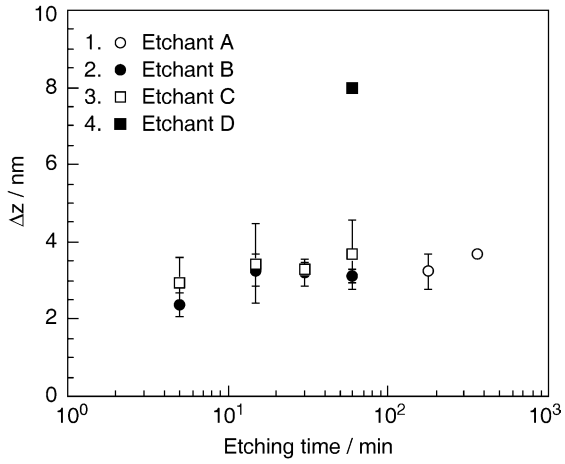

Fig. 3. Height difference at the boundary between etched and intact regions as a function of etching time using various etchants.

account that evanescent waves are exponentially attenuated from the outermost surface, the ideal thickness of the surface amorphous layer could be calculated. The value so obtained was 1.6 nm, and was approximately a half of the experimental result from the surface etching treatment. This means that in the real experiment, the analytical depth for GIXD was deeper than the calculation due to the surface roughness, although the essential discussion after the GIXD measurements will not be altered.

The iPP films used here were melt-quenched, as stated in Section 2. In general, annealing of crystalline polymers at a temperature slightly lower than the melting point, so-called isothermal crystallization, induces thickening of crystalline lamellae. If the lamellae beneath the surface amorphous layer become thicker, the surface amorphous layer might get thinner. Hence, it was examined how the thickness of the surface amorphous layer changes after isothermal crystallization at various temperatures for 24 h. Fig. 4 shows the result. The thickness slightly decreased with increasing crystallization temperature, and reached a constant value of 2.7 ± 0.7 nm after 413 K. This indicates that the film surface even for the iPP, being in a quasi-equilibrium state, is covered with the amorphous phase.

3.2. Surface molecular motion

We now turn to surface dynamics in the iPP films using LFM. The origin of lateral force is closely related to energy dissipation during tip sliding [37,38]. Hence, the relation between temperature and lateral force can be regarded as temperature dependence of loss modulus (E'') at the surface. At first, the difference of surface molecular motion between the intact and etched regions in the iPP thick film [39] was discussed. Fig. 5 shows the temperature dependence of lateral force for the iPP film, which was in part treated by the permanganate solution. In the case of the intact region, a significant lateral force peak arisen from a relaxation process was observed at about 250 K. On the other hand, in the case of the etched region, lateral force was almost invariant with respect to measuring temperature. What is the difference between the two is whether the surface amorphous layer is existed. Thus, it can be envisaged that the relaxation peak observed in the intact region is originated from the surface amorphous layer. We define this surface α_a-relaxation process.

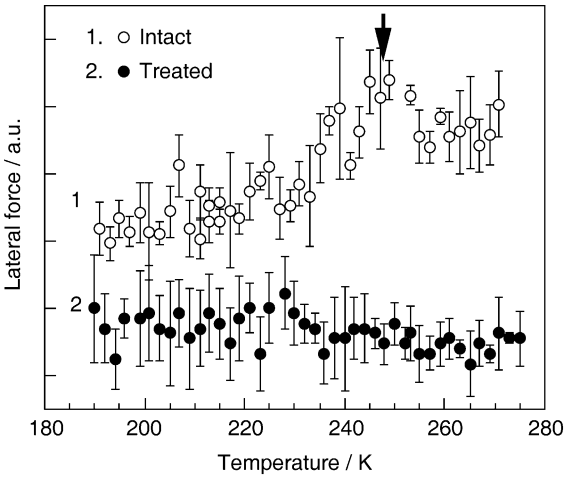

Fig. 5. Temperature dependence of lateral force for intact and etched regions in the iPP film. The measurements were made at the scanning rate of 1 μm s^{-1}.

Then, the surface mobility is compared with the bulk one. Fig. 6 shows the temperature dependences of lateral force and bulk E''. LFM data presented was obtained from the intact surface region, being imported from Fig. 5. The scanning rate for the measurement was 1 μm s^{-1}. Since this value was simply converted to the frequency of 78 Hz [37], the LFM data can be directly compared with the bulk data at 70 Hz. On the temperature–bulk E'' curve, the α_a-absorption peak corresponding to the segmental motion in the

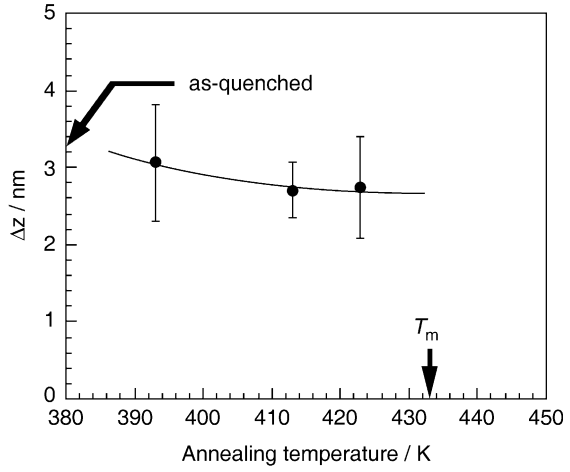

Fig. 4. Height difference at the boundary between etched and intact regions after various isothermal crystallizations. The curve was drawn to guide the eye.

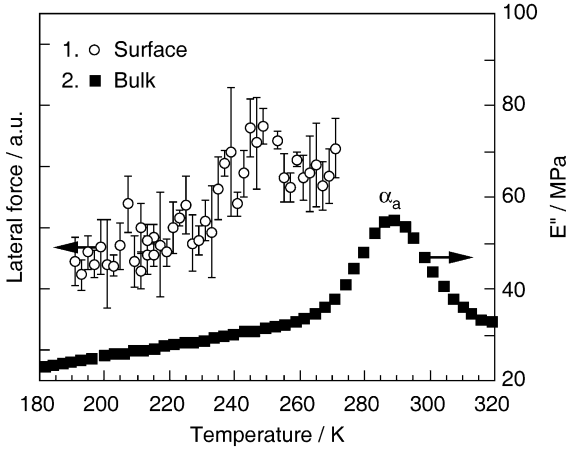

Fig. 6. Temperature dependences of lateral force and bulk E'' for the iPP film. The lateral force data was adapted from Fig. 5. The bulk data was acquired at the frequency of 70 Hz.

amorphous region was discernibly observed at approximately 285 K. A similar peak was also observed at the surface, but the observed temperature was approximately 250 K, which was much lower than the corresponding bulk value. Fig. 7 shows the temperature dependences of lateral force and bulk E'' as a function of frequency (f) for the iPP. The peak was observed for all frequencies and was shifted to the higher temperature side with increasing frequency. This inclination was seen for the surface as well as the bulk. In the case of the bulk measurement with lower frequencies, an additional relaxation process was observed at a higher temperature side. This has been widely accepted as a crystalline relaxation process [40]. However, it could be hardly concluded whether the crystalline relaxation process was present at the surface. This was because once measuring temperature went beyond the surface α_a-relaxation temperature, the surface became so sticky, resulting in truncation of the measurement, as seen in Fig. 7.

Invoking that the relation between frequency and reciprocal number of peak temperature (T_{max}) is Arrhenius-type, apparent activation energy ($\Delta H^{\ddagger}$) for the relaxation process can be obtained by the following equation

$$\Delta H^{\ddagger} = -R\{\mathrm{d}(\ln f)/\mathrm{d}(T_{max})\} \quad (3)$$

where R is the gas constant. Fig. 8 shows such the plots. The relation between $1/T_{max}$ and $\ln f$ was apparently linear for both. The $\Delta H^{\ddagger}$ values for the surface and bulk relaxation processes were estimated on the basis of the slopes as 230 ± 10 and 380 ± 20 kJ mol^{-1}, respectively.

For the iPP, the observed surface $\Delta H^{\ddagger}$ value was lower than the corresponding bulk value. In addition, the surface

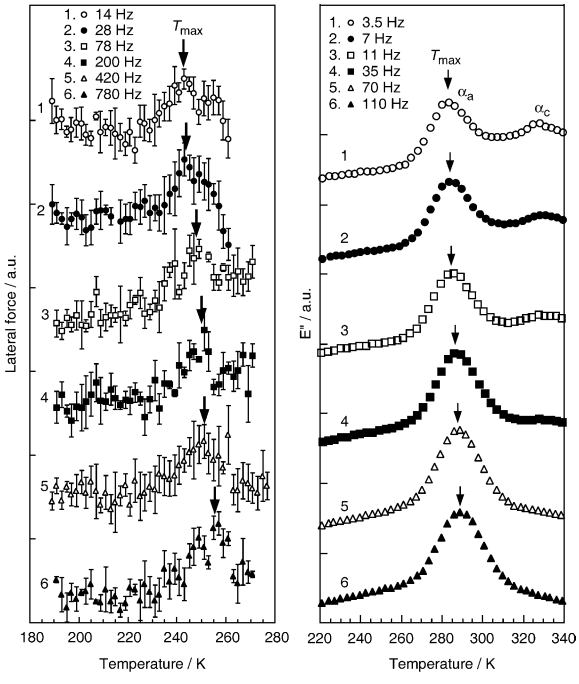

Fig. 7. Temperature dependences of lateral force and bulk E'' as a function of frequency for the iPP film.

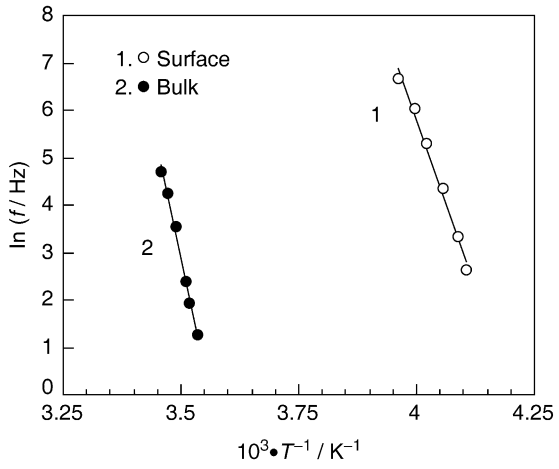

Fig. 8. Relation between logarithmic frequency and reciprocal number of T_{max}.

relaxation temperature was lower than the corresponding bulk one, as shown in Fig. 6. These results make it clear that surface mobility is much more enhanced than the bulk one even in the semi-crystalline iPP film. This conclusion is the same as what we have seen for surface molecular motion in amorphous atactic PP films [41], and is in good accordance with simulation results [42,43].

3.3. Film with thinner surface amorphous layer

So far, we have successfully presented how surface mobility differs from the bulk one for the iPP films. However, we have not seen any features that the sample is in a semi-crystalline state. This might be because the surface amorphous layer is quite thick as 3.3 nm. If we are able to prepare an iPP film with a thinner surface amorphous layer, surface mobility might be restricted by the underneath crystalline phase. Thus, the iPP-NaCl film was prepared.

The thickness of the surface amorphous layer in the iPP-NaCl film was examined by the same procedure, as mentioned above. To do so, the etchant solution B was used and was allowed to oxidize the surface for 30 min. This should be the most appropriate condition to strip only the surface amorphous layer off from the iPP film. The part (a) of Fig. 9 shows the optical micrograph of the iPP-NaCl film on which a droplet of the etchant solution was put. The darker area on the left-hand side corresponds to the droplet. After the droplet was taken away, the surface was thoroughly washed with pure water, and was observed by AFM. The part (b) of Fig. 9 is the surface topographic image. The height difference between etched and intact regions was observed, as indicated by arrows, although it was not so easy to identify. This was because the height difference formed after the etching treatment was lower than other steps, which was transcribed from surface steps of the NaCl crystal. Since we, using a CCD camera, monitored where the droplet was, the border between etched and intact

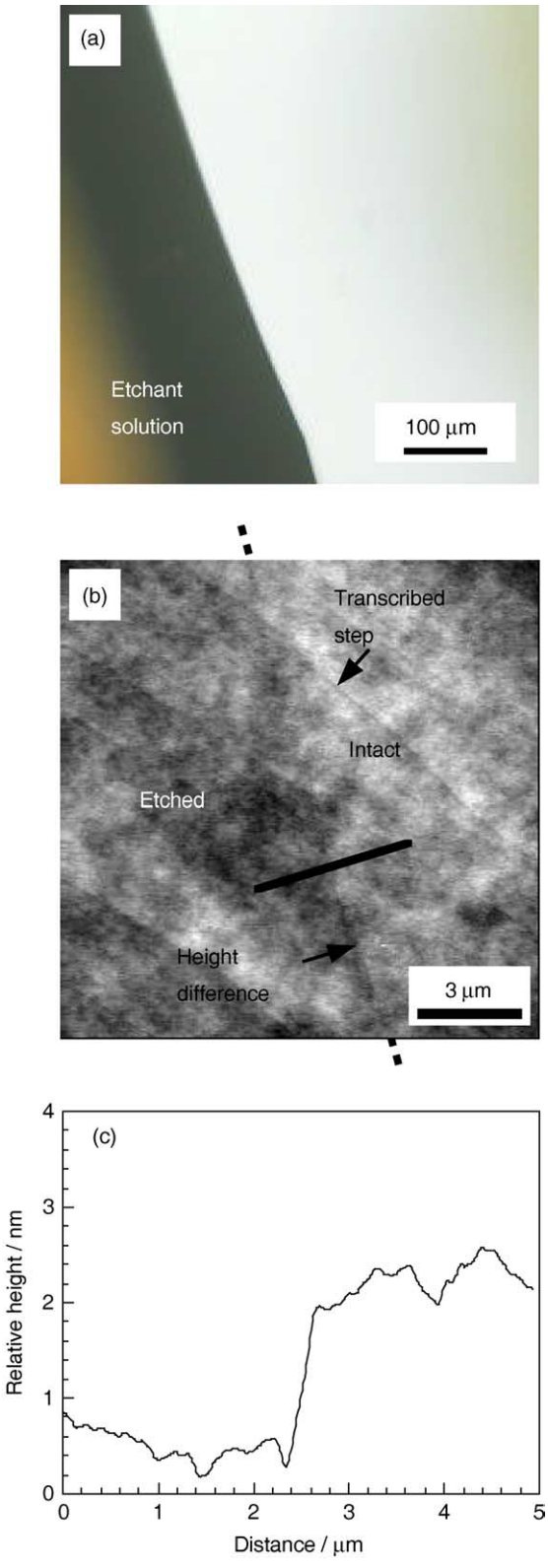

Fig. 9. (a) Optical microscopic image of the iPP-NaCl film on which a droplet of the etchant was put, (b) topographic image at the boundary between etched and intact regions, and (c) height profile along the line in (b).

regions could be addressed. Fig. 9(c) illustrates the height profile along the line drawn in the AFM image. The step height between the two regions was 1.5 ± 0.4 nm, which was approximately a half of the surface layer in the iPP films prepared without NaCl. On the film preparation process, the iPP melt was contacted with the NaCl crystal. Hence, possibilities of transcrystallization and/or epitaxial growth of iPP chains at the interface were here considered. The lattice spacing of (001) face for the NaCl crystal is 0.563 nm. Although this does not match to any spacing for the iPP crystal with the α form, some examples of epitaxial growth of the iPP chains on the NaCl crystal from a dilute solution was reported by Koutsky et al. [44]. However, they also pointed out that epitaxial growth of the iPP chains was much more difficult than other polymers. In fact, no features of crystalline structure were observed at the iPP-NaCl film surface, as shown in Fig. 9(b). Thus, it seems reasonable to assume that the difference of surface structure between the iPP and iPP-NaCl films is only the thickness of the surface amorphous layer. In addition, the iPP-NaCl film was dried at room temperature, which was far above T_g^b, for an approximately week. Thus, even if the surface was stressed upon the film preparation process with NaCl, it must be fully relaxed.

We finally come to thermal molecular motion at the surface in the iPP-NaCl film. Fig. 10 shows the temperature dependence of lateral force for the iPP-NaCl film. For a comparison, the data for the iPP film, which was already presented in Fig. 5 [45], was also shown. A clear lateral force peak was similarly observed even in the iPP-NaCl film. However, the peak temperature was shifted to higher by about 10 K, although the value was still lower than the

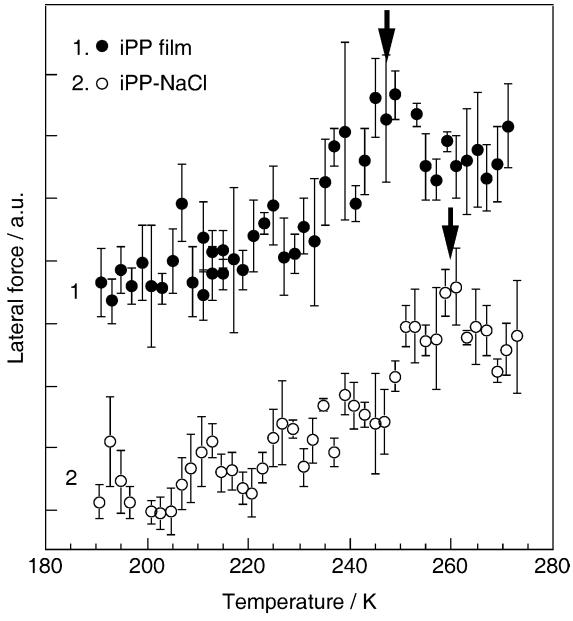

Fig. 10. Temperature dependence of lateral force for the iPP-NaCl film. For a comparison, the same relation for the iPP film is also presented by adapting from Fig. 5.

corresponding bulk one. In other words, mobility at the surface in the iPP-NaCl film was enhanced in comparison with that in the bulk, but the extent was not as much as the iPP film surface. This implies that molecular motion in the surface amorphous phase of the iPP-NaCl film is restricted by the underneath crystalline phase. So far, the characteristic length scale of cooperative segmental motion has been extensively studied. Consequently, the value near the transition temperature seems to be a few of nanometers [46,47]. If this is the case, the surface amorphous layer in the iPP-NaCl film is supposed to be thinner than the characteristic length, meaning that surface mobility in the iPP-NaCl film is interfered by the underneath crystalline phase. In a sense, this experiment might enable us to discuss about the characteristic length scale for the cooperative segmental motion.

4. Conclusions

Semi-crystalline films of iPP were prepared by a melt-quenching method. Apparent crystallinity in the surface region was lower than that in the bulk. The iPP surface was covered with the 3 nm thick amorphous layer. Surface α_a-relaxation process was observed at about 250 K, and its apparent activation energy was 230 ± 10 kJ mol^{-1}. Both were lower than the corresponding bulk values. When the surface amorphous layer became thinner, the surface α_a-relaxation temperature increased due probably to an effect of underneath crystalline phase.

Acknowledgements

We are most grateful for fruitful discussion with Prof. Atsushi Takahara, Kyushu University and Dr. Sono Sasaki, JASRI. We greatly thank Mr. Yuji Fujita, Japan Polychem Corporation, for his gift of the iPP sample. This was in part supported by a Grant-in-Aid for the 21st century COE program 'Functional Innovation of Molecular Informatics' from the Ministry of Education, Science, Sports, and Culture, Japan, and by Matsuda Science Foundation.

References

[1] Andrade JD. Surface and interfacial aspects of biomedical polymers. New York: Plenum Press; 1985.
[2] Garbassi F, Morra M, Occhiello E. Polymer surfaces from physics to technology. Chichester: Wiley; 1994.
[3] Meyers GF, DeKoven BM, Seitz JT. Langmuir 1992;8:2330–5.
[4] (a) Reiter G. Europhys Lett 1993;23:579–84.
(b) Reiter G. Macromolecules 1994;27:3046–52.
[5] (a) Kajiyama T, Tanaka K, Ohki I, Ge SR, Yoon JS, Takahara A. Macromolecules 1994;27:7932–4.
(b) Tanaka K, Takahara A, Kajiyama T. Macromolecules 2000;33:7588–93.
[6] (a) Keddie JL, Jones RAL, Cory RA. Europhys Lett 1994;27:59–64.
(b) Kawana S, Jones RAL. Phys Rev E 2001;63:021501.
[7] (a) Forrest JA, Dalnoki-Veress K, Stevens JR, Dutcher JR. Phys Rev Lett 1996;77:2002–5.
(b) Forrest JA, Dalnoki-Veress K, Dutcher JR. Phys Rev E 1997;56:5705–16.
[8] Jean YC, Zhang RW, Cao H, Yuan JP, Huang CM, Nielsen B, Asoka-Kumar P. Phys Rev B 1997;56:R8459–R62.
[9] DeMaggio GB, Frieze WE, Gidley DW, Zhu M, Hristov HA, Yee AF. Phys Rev Lett 1997;78:1524–7.
[10] (a) Agra DMG, Schwab AD, Kim JH, Kumar S, Dhinojwala A. Europhys Lett 2000;51:655–60.
(b) Schwab AD, Agra DMG, Kim JH, Kumar S, Dhinojwala A. Macromolecules 2000;33:4903–9.
[11] (a) Hall DB, Torkelson JM. Macromolecules 1998;31:8817–25.
(b) Ellison CJ, Torkelson JM. Nat Mater 2003;2:695–700.
[12] Fryer DS, Nealey PF, de Pablo JJ. Macromolecules 2000;33:6439–47.
[13] Kerle T, Lin ZQ, Kim HC, Russell TP. Macromolecules 2001;34:3484–92.
[14] (a) Wallace WE, Fischer DA, Efimenko K, Wu WL, Genzer J. Macromolecules 2001;34:5081–2.
(b) Wu WL, Sambasivan S, Wang CY, Wallace WE, Genzer J, Fischer DA. Eur Phys J E 2003;12:127–32.
[15] Fischer H. Macromolecules 2002;35:3592–5.
[16] Bliznyuk VN, Assender HE, Briggs GAD. Macromolecules 2002;35:6613–22.
[17] (a) Forrest JA, Mattsson J, Borjesson L. Eur Phys J E 2002;8:129–36.
(b) Teichroeb JH, Forrest JA. Phys Rev Lett 2003;91:016104.
[18] Weber R, Grotkopp I, Stettner J, Tolan M, Press W. Macromolecules 2003;36:9100–6.
[19] Hamdorf M, Johannsmann DJ. Chem Phys 2000;112:4262–70.
[20] (a) Ge S, Pu Y, Ahang W, Rafailovich M, Sokolov J, Buenviaje C, Buckmaster R, Overney RM. Phys Rev Lett 2000;85:2340–3.
(b) Pu Y, Ge S, Rafailovich M, Sokolov J, Duan Y, Pearce E, Zaitsev V, Schwarz SA. Langmuir 2001;17:5865–71.
[21] Weber R, Zimmermann KM, Tolan M, Stettner J, Press W. Phys Rev E 2001;64:061508.
[22] Galli P, Vecellio G. Prog. Polym. Sci. 2001;26:1287–336.
[23] (a) Magonov SN, Qvarnstrom K, Elings V, Cantow HJ. Polym Bull 1991;25:689–94.
(b) Stocker W, Magonov SN, Cantow HJ, Wittmann JC, Lotz B. Macromolecules 1993;26:5915–23.
(c) Magonov SN, Reneker DH. Annu Rev Mater Sci 1997;27:175–222.
[24] (a) Schonherr H, Snetivy D, Vancso GJ. Polym Bull 1993;30:567–74.
(b) Vancso GJ, Nisman R, Snetivy D, Schonherr H, Smith P, Ng C, Yang HF. Colloids Surf A 1994;87:263–75.
[25] Sasaki S, Sakaki Y, Takahara A, Kajiyama T. Polymer 2002;43:3441–6.
[26] (a) Kawamoto N, Mori H, Nitta K, Sasaki S, Yui N, Terano M. Macromol Chem Phys 1998;199:261–6.
(b) Kawamoto N, Mori H, Nitta K, Yui N, Terano M. Angew Makromol Chem 1998;256:69–74.
[27] Nishino T, Matsumoto T, Nakamae K. Polym Eng Sci 2000;40:336–43.
[28] Yakabe H, Sasaki S, Sakata O, Takahara A, Kajiyama T. Macromolecules 2003;36:5905–7.
[29] Dosch H. Critical phenomena at surfaces and interfaces, evanescent X-ray and neutron scattering. Berlin: Springer; 1992.
[30] Factor BJ, Russell TP, Toney MF. Macromolecules 1993;26:2847–59.
[31] Gracias DH, Zhang D, Lianos L, Ibach W, Shen YR, Somorjai GA. Chem Phys 1999;245:277–84.
[32] Uedono A, Suzuki R, Ohdaira T, Mikado T, Tanigawa S, Ban M, Kyoto M, Uozumi T. J Polym Sci, B: Polym Phys 2000;38:101–7.
[33] Kawamoto N, Mori H, Yui N, Nitta KH, Terano M. Angew Makromol Chem 1996;243:87–98.
[34] Norton DR, Keller A. Polymer 1985;26:704–16.

[35] Natta G, Corradini P, Cesari M. Rend Accad Naz Lincei 1957;22: 11–17.
[36] In this case, the sample surface is not necessarily flat, although a flatter surface is better to evaluate step heights. However, if a strong etchant was used, the thin films with a flatter surface were sometimes so corrosive and a part of the film was broken up. In addition, it was experimentally easy to prepare the thick films for the iPP used. Thus, we here used the iPP thick films. The same experiment was also performed for the 170 nm thick film, and the result was in agreement with that in the thick film within our experimental accuracy.
[37] Kajiyama T, Tanaka K, Takahara A. Macromolecules 1997;30:280–5.
[38] Hammerschmidt JA, Gladfelter WL, Haugstad G. Macromolecules 1999;32:3360–7.
[39] The measurement was also made on the 170 nm thick film, and the result was in good accordance with the data shown in Fig. 5.
[40] Takayanagi M, Hoashi K, Minami S, Yasuda H. Rep Prog Polym Phys Jpn 1963;6:121–4.
[41] Sakai A, Tanaka K, Kajiyama T, Takahara T. Polymer 2002;43: 5109–15.
[42] Mansfield KF, Theodorou DN. Macromolecules 1991;24:6283–94.
[43] Doruker P, Mattice WL. J Phys Chem B 1999;103:178–83.
[44] Koutsky JA, Walton AG, Baer E. J Polym Sci, A-2 1966;4:611–29.
[45] We also examined surface relaxation behavior in an iPP film with 2.7 nm thick surface amorphous layer. In this case, surface relaxation temperature was the same as that for the iPP film with 3.3 nm thick surface layer.
[46] Donth E. J Non-Cryst Solids 1982;53:325–30.
[47] Ediger MD. Annu Rev Phys Chem 2000;51:99–128.